LA-UR-08-4295

Approved for public release; distribution is unlimited.

Title:	Formation and dynamics of supported phospholipid membranes on a periodic nanotextured substrate
Author(s):	James H. Werner, Gabriel A. Montaño, Agnes A. Zurek, Elshan A. Akhadov, Anthony L. Garcia, Gabriel P. Lopez, and Andrew P. Shreve
Intended for:	Publication/submission to Langmuir

Los Alamos
NATIONAL LABORATORY
EST. 1943

Form 836 (7/06)

Formation and dynamics of supported phospholipid membranes on a periodic nanotextured substrate

James H. Werner[†*], Gabriel A. Montaño[†], Agnes A. Zurek[†], Elshan A. Akhadov[†], Anthony L. Garcia[§], Gabriel P. Lopez[§*], and Andrew P. Shreve[†*]

Abstract

We have studied and modeled the morphology and dynamics of planar lipid bilayer assemblies supported on a textured silicon substrate that contains nano-structured features perpendicular to the plane of observation. Using a combination of characterization methods, including atomic force microscopy and quantitative fluorescence microscopy, we have discovered the bilayer assemblies are conformal to the underlying nanostructured substrate. As far as the dynamics are concnerned, the lipids freely diffuse in and out of the plane of observation while supported by the nanotextured material. In a microscopic sense, diffusion is isotropic along the patterned substrate. Macroscopically, when observed over length scales exceeding the dimensions of the nano-structured features, the diffusion appears anisotropic. The observed macroscopic anisotropy is well simulated using models of diffusion on the nanostructured surface that assume the lipids diffuse homogeneously and isotropically on the supporting nanotextured substrate.

*Email: JHW: jwerner@lanl.gov; GPL: gplopez@unm.edu; APS: shreve@lanl.gov

[†]Center for Integrated Nanotechnologies, Materials Physics and Application Division, Los Alamos National Laboratory, Los Alamos, NM 87545

[§]Department of Chemical and Nuclear Engineering, Center for Biomedical Engineering, 209 Farris Engineering Center, University of New Mexico, Albuquerque, NM 87131

Current addresses: AAZ: Nesia's address; EAA: Elshan's address

Introduction.

Supported planar lipid bilayers are important model systems enabling the control, organization and study of membranes and membrane-associated proteins.[1] In addition to fundamental biophysical investigations, supported bilayers are useful scaffolds for many practical applications, such as electrophoretic separations[2, 3] or protein recognition arrays[4, 5]. For many of these applications, there is often a need to physically segregate and isolate sections of planar lipid bilayers on nanometer to micron length scales. To this end, patterning methods directly taken from microelectronics, such as micro-contact printing and stamping techniques[6-10] or photolithographic methods[11-13], have seen widespread use for containing and controlling lipid domains in two spatial dimensions.

While methods to control and characterize the interaction of planar lipid bilayers with nano and micro structured surfaces in two dimensions are rather well established, a handful of recent experimental investigations have also begun to address the interaction of planar lipid bilayers with substrates that demonstrate texture or patterning in three spatial dimensions on nanometer to micron length scales.[14, 15] For example, Parthasaranthy, Yu, and Groves[14] studied the phase segregation of lipid/cholesterol mixtures in double bilayer assemblies formed on a solid support that was spatially patterned with micron-scale rounded stripes that protruded several hundred nanometers from the surface. This study discovered that phase segregation was critically dependent upon the local curvature. In another recent study that explored the interaction of planar lipid bilayers with nano-structured 3D surfaces, Lopez and coworkers[15] found that mixtures of long- and short-chain lipids in an appropriate concentration ratio formed micron-scale bilayer assemblies (bicelles) capable of spanning hundred nanometer-sized troughs on nanostructured silicon.

For both fundamental research concerning lipid organization and for applications such as trans-membrane protein separation technologies[2] it is important to understand the interactions between textured substrates and the adhered lipid assemblies. One desires characterization methods that can study lipid morphology on multiple length scales both in and out of the plane of observation. Here, we demonstrate various methods of characterizing lipid bilayers and their

adherence to simple, three dimensionally nano-structured substrates. Atomic force microscopy (AFM), scanning electron microscopy of the underlying substrate, as well as a standard optical measure of membrane diffusivity, fluorescence recovery after photobleaching, FRAP, are used to characterize a planar lipid bilayer assembly supported on a three dimensionally nano-structured surface. While FRAP, like fluorescence microscopy, is generally a technique limited in spatial resolution to the wavelength of light used for observation, we show here that a detailed analysis of the recovery after photobleaching can be used to infer the nano-morphology of the lipid bilayer. For the membrane compositions, surfaces, and environmental conditions used here, the FRAP and AFM measurements both demonstrate that the lipid bilayer is conformal to the underlying nano-structured surface.

Materials and Methods.

Silicon Wafers. Oxidized flat silicon wafers were obtained from NOVA Electronic Materials, Ltd. (Carrollton, TX), and were textured using interferometric lithography, as previously described.[15, 16] Prior to use, the wafers were cleaned by exposure to intense deep-uv light (185 to 254 nm) for up to 90 minutes.

Vesicle preparation and Supported Lipid bilayer formation. 1-Palmitoyl-2-oleoyl-*sn*-glycero-3-phosphocholine (POPC) was purchased in powder form from Avanti Polar Lipids and 1,2 dihexadecanoyl-*sn*-glycero-3-phosphoethanolamine, triethylammonium salt (Texas Red DHPE) was purchased from Invitrogen. Lipid solutions were made in chloroform (Sigma) and stored at 4° C. 1 mg/ml concentrations of POPC were used and in the case of FRAP studies the lipid solution contained 0.2-0.5 lipid mole % of Texas Red DHPE. To create liposome solutions, a small amount of lipid in chloroform is dried under Argon gas and re-suspended in 100 mM phosphate buffered saline solution at pH 7.4 (Sigma). A solubilized liposome solution was created by freeze-thawing three times using liquid nitrogen. Uniform liposome preparations were created using a mini-extruder (Avanti) with 0.1 μm pore-size polycarbonate membranes. Lipid bilayers were formed by placing a 25μl aliquot of 1 mg/ml liposome solution on a Petri dish and placing the nanostructured surface face down on the solution. After 15 min., the sample is placed

in a doubly-distilled H_20 reservoir, turned over and gently rinsed in the reservoir prior to FRAP and AFM analysis.

SEM of grooved silicon grating. High resolution Scanning Electron Microscopy images were obtained using a Quanta 400 FEG from FEI Company. Images were obtained in vacuum. Prior to imaging, the substrate was cleaned in a UV/Ozone environment for 10 min.

Atomic Force Microscopy. All AFM images were performed using a Molecular Imaging Pico Plus II Atomic Force Microscope in MAC mode using standard MAC II cantilevers and operated at resonance frequencies in air of ~70 kHz and in liquid at ~20-35 kHz. Images were obtained at scan rates of ~1-1.5 Hz.

Fluorescence Recovery After Photobleaching (FRAP). FRAP experiments were performed using an Olympus IX-81 inverted optical microscope equipped with an Orca 3-CCD camera (Hamamatsu, C7780-20). Bleaching was performed by using a 50x objective and narrowing the iris to produce a small circular initial bleached area. Subsequent images were taken using automated software allowing opening of the shutter for only enough time to obtain an image, thus reducing any long-term photobleaching effect. Images were obtained once per minute.

FRAP Analysis. Fluorescence recovery after photobleaching is governed by the two dimensional diffusion equation.[17] In our case, the diffusion coefficient for molecules diffusing parallel or perpendicular to the grooved surface appear, macroscopically, to be different (see Results and Discussion sections). To account for this anisotropy in the macroscopic diffusion, the fluorescence recovery after photobleaching is modeled using a two-dimensional diffusion equation (Eqn. 1) that has different diffusion coefficients for the directions parallel or perpendicular to the grooves in the surface:

$$D_x \frac{\partial^2 c}{\partial x^2} + D_y \frac{\partial^2 c}{\partial y^2} = \frac{\partial c}{\partial t} \qquad (1)$$

In the above equation, c denotes the concentration of the fluorescent lipid and the coordinate system has been rotated such that the x and y axes are parallel with the principle diffusion axes (e.g. the x-direction is parallel to the grooves and the y-direction is perpendicular to them).

Assuming the concentration of fluorescent molecules following the bleach can be adequately described as a Gaussian (Eqn. 2),

$$c(x,y,t=0)=c_{\infty}\left(1-\alpha\cdot\exp\left(-\frac{x^2}{2\sigma_{x0}^{\,2}}\right)\cdot\exp\left(-\frac{y^2}{2\sigma_{y0}^{\,2}}\right)\right) \tag{2}$$

then, Eqn. 1 can be solved by a Fourier Transform method, with the concentration of fluorescent lipid as a function of time being given by:

$$c(x,y,t)=c_{\infty}\left(1-\alpha\cdot\frac{\sigma_{x0}\sigma_{y0}}{\sigma_x(t)\ \sigma_y(t)}\exp\left(-\frac{x^2}{2\sigma_x(t)^2}\right)\cdot\exp\left(-\frac{y^2}{2\sigma_y(t)^2}\right)\right) \tag{3}$$

In Eqn. 2 and 3, c_{∞} denotes the concentration of the fluorescent lipid unperturbed by a bleach, α is a value ranging between 0 to 1 to reflect the "depth" of the bleach, σ_{x0} is the standard deviation of the initial bleach in the x-direction at t = 0 and σ_{y0} is the standard deviation of the initial bleach in the y direction. The variables $\sigma_x(t)$ and $\sigma_y(t)$ describe how the initial Gaussian bleach widens over time and are given by:

$$\sigma_x^2(t)=\sigma_{x0}^2+2\cdot D_x\cdot t;\qquad \sigma_y^2(t)=\sigma_{y0}^2+2\cdot D_y\cdot t \tag{4}$$

To determine D_x and D_y from the photobleaching recovery, we fit successive frames of the photobleaching movies to an elliptical Gaussian (Eqn. 3, with $\sigma_x(t)$, $\sigma_y(t)$ treated as freely floating variables in the fit function (fitting done by chi-squared minimization in Igor Pro (Wavemetrics, Lake Oswego, OR). A plot of the standard deviation squared for either of the

principle axes obtained from the fits to the data versus time should be linear, with a slope of twice the diffusion coefficient for that axis.

Results.

SEM, AFM and light diffraction experiments were used to determine the dimensions, morpohology and condition of the nanostructured surfaces. From SEM micrographs, the wells were determined to be 320 nm deep with a width of 160 nm and an average periodicity of 522 nm (Fig. 1). An oxide layer can also be observed as the lighter contrasting portion of the structure that tracks along the outer portion of the structured material. Figure 2a is a 3D rendering of an AFM topography image of the nanostructured surface. The 2D topography image is shown in the inset. The nanostructured surface is very smooth and free of debris. The uniformity and periodicity of the nanostructured substrate is apparent in Figure 2c. The spacing between the centers of the nanostructured throughs in this image is ≈530 nm, in close agreement with the SEM results (Fig. 1). However, due to the nature of the tip shape and depth of the wells, accurate depths and distances between steps are not attainable from AFM results, in contrast to the SEM measurements. This limitation of AFM is commonly encountered in imaging high-aspect ratio structures such as these. As another independent probe of the nature of the textured surface, we measured the diffraction of light from the grating-like surfaces for several incident angles (data not shown), and analyzed the observed diffraction angle using a standard grating equation. This analysis indicates that the periodicity of the surface texture is 518 ± 4 nm, in quantitative agreement with the SEM analysis. Thus, SEM, AFM and light diffraction methods all produce consistent results in terms of the dimensions of the textured surfaces.

AFM of the nanostructures incubated with POPC indicates formation of a bilayer that appears to conform tightly to the surface (Figure 2b). The width (full-width at half maximum) of the raised structures in the images increases from 419 nm to 431 nm, presumably due to the presence of the lipid (Figure 2d). This increase is consistent with the presence of a lipid bilayer on either side of the structure, thereby increasing the total thickness of each structure by effectively two bilayers. There also appears to be a decrease in the depth of the wells in the presence of the lipids, however, this change is also likely influenced by the tip geometry and an

inability to completely insert the tip into the wells. Therefore, this decrease of depth is considered to be related to the increased thickness due to the lipid bilayer, rather than indicating that the bilayer is not conforming to the wells.

In order to characterize the fluidity of the lipid bilayers formed on the nanostructured surface, we performed fluorescence recovery after photobleaching. Figure 3a shows recovery of a bleached area of bilayer. The line represents the long axis of the grooves in the substrate. Initially, the bleached area is circular. Over time, fluidity of the lipids causes unbleached lipid to diffuse into the bleached area and bleached lipid to diffuse out of the bleached spot. However, while the surface recovers from bleaching, the diffusive recovery observed is not typical. In general, the recovery of a circular beach is isotropic and the image at any given instant retains radial symmetry. Here, instead of recovering at an equal rate in all dimensions, recovery is faster along one axis than the other: the fluorescence image over time becomes elliptical rather than circular, due to a quicker recovery along the axis of the grooves in the substrate (D_x), and a slower recovery perpendicular to the grooves in the substrate (D_y) (Figure 3b). This particular bleach recovery was fit using Eqn 3 to obtain values for both D_x and D_y, yielding diffusion constants of 0.76 and 0.18 $\mu m^2/s$ respectively (see Fig. 4a). These values reflect an effectively faster diffusion along the length of the grooves relative to that perpendicular to the grooves, with a corresponding increase in diffusion coefficients of a factor of 4.2. Averaging the results of analysis of multiple experiments yields a ratio of diffusion coefficients of 4.3 ± 0.2, with a corresponding slow diffusion coefficient of 0.21 μm^2/sec and a fast diffusion coefficient of 0.90 μm^2/sec. Comparison of these results to simulated diffusional behavior is described in the Discussion section.

Discussion.

The formation of substrate-supported POPC bilayers that are conformal with the textured substrate is validated by the results of the experimental results reported above. AFM experiments carried out using high resolution tips provide an indication that the membranes are invaginated into the grooves of the substrate: the observed width of the grooves in the presence and absence of the phospholipid differs by about 12 nm, a value consistent with the narrowing of the effective

groove by the presence of two lipid bilayers, one on either side of the groove. However, AFM is unable to image to the full groove depth, and so leaves unresolved whether or not the membranes are fully conformal with the contours of the substrate. In order to begin to address this question, quantitative fluorescence microscopy techniques can be applied.

In fluorescence recovery after photobleaching (FRAP) measurements, a striking anisotropy in diffusion constants is observed in directions parallel to and perpendicular to the groove direction. In principle, two possible effects could contribute to such anisotropy. One would be that the textured surface inhibits diffusion in the direction perpendicular to the grooves, whether for a membrane that is conformal to the surface or for one that is suspended above the groove, and the second is that a membrane conformal (or nearly so) to the grooved substrate demonstrates a smaller effective diffusion coefficient perpendicular to the grooves simply because the diffusing molecules must traverse a longer distance on the surface than is observed in the image plane. We first note that a suspended membrane is inconsistent with the AFM images, which clearly demonstrate that the membrane is at least partially conformal with the topology of the substrate. We also note that the diffusion coefficient along the "fast" axis of the anisotropic diffusion is near 1 μm^2/sec, or nearly equal to that observed for typical supported bilayers of POPC on silica surfaces. Thus, along one axis, there is no indication that the nature of the textured surface influences diffusive behavior. A plausible explanation for the observed anisotropy remains that the effective observed diffusion for a membrane conformal to the surface should be reduced in the direction perpendicular to the grooves because the diffusing molecules have to travel further than is observed in the image plane in order to traverse the vertical regions of the grooves. In order to explore whether this explanation is valid and also to what degree the FRAP experiments provide evidence for a nearly conformal membrane on the surface, we next consider a detailed, quantitative analysis of a diffusion process and a FRAP experiment on a textured (grooved) surface.

It is possible to relate the observed ratio in the diffusion coefficients to the underlying morphology of the surface. Figure 5 is an illustration of the periodic nanostructured substrate similar to the SEM image shown in Figure 1. For molecules that are traveling by Brownian motion on this surface, there are 2 principal directions for diffusion, parallel or perpendicular to

the grooves. Molecules traveling parallel to the grooves would appear to diffuse "normally," as a molecule that travels an actual distance "d" on the surface in this direction also appears macroscopically to have traveled a distance "d" in this direction. However, for the motion of a molecule in the direction perpendicular to the grooves, the apparent diffusion coefficient is slower. This slowing reflects the fact that a molecule travelling in this direction does not appear to cover as much macroscopically observable distance as it actually travels, for part of the motion involves moving up and down the grooves of the surface. The time involved to move diffusively across a single period of the grating (a unit cell, see Fig. 5), for the grooved substrate would scale as $t \sim \frac{(a+2b+c)^2}{D}$. Alternatively, if the molecule did not have to go up and down the vertical parts of the surface in this direction, the time to go across a unit cell would scale as $t \sim \frac{(a+c)^2}{D}$. Thus, one might expect the "apparent" diffusion coefficient, D_{app}, in this dimension to scale as the ratio of these times, e.g.:

$$D_{app} \approx \frac{(a+c)^2}{(a+2b+c)^2} D \tag{5}$$

As b tends to zero or infinity, the above relation reaches the expected asymptotic values of $D_{app} \approx D$ and $D_{app} \approx 0$, respectively. Note that this simple model compares time (and not distances) across a "grooved" or "flat" (*i.e.*, b=0) unit cell, and thus scales as the squares of the distances, as appropriate for diffusional behavior. Using the dimensions of the surface determined by SEM (a≈360 nm, b≈320 nm, c≈160 nm), Equation 5 yields D_{app} equal to ~0.2*D. Thus, the ratio obtained from this simple model, (D/D_{app}), is ~5, in reasonable agreement with the measured diffusion ratio, 4.3 ± 0.2. Nevertheless, there are several approximations used in this simple analysis of the FRAP data that could influence the validity of this comparison, so a more detailed analysis is next considered.

One may question whether Equations 1-4 adequately model the diffusion on these surfaces. For example, can the concentration profile on these surfaces following a bleach be approximated as a Gaussian? Since molecules on the vertical portions of the surface all should have approximately the same probability to be bleached, the underlying concentration of

fluorescent molecules is inherently "banded" at the beginning of the recovery. Moreover, the number of fluorescent lipids observed in the x-y plane is a periodic function along the direction perpendicular to the grooved surface (it is larger at every wall of the grooved surface), and is not clamped at a fixed value c_∞. However, since we observe the surface at visible wavelengths (excitation light of ~ 600 nm) through a 0.45 numerical aperture (NA) objective, spikes in fluorescent lipid concentration are effectively "smeared-out" due to diffraction. Further, the finite size of the CCD pixels (each pixel in the FRAP image corresponds to a box of ~ 0.6 μm sides) also blurs out the underlying spatial periodicity. Equations 1-4 take in account neither the non-Gaussian nature of the initial bleach nor the fact the underlying concentration of fluorescent lipids is non-uniform in one spatial dimension.

In order to test the impact of the above issues on the measured data, we constructed a simulation to model the macroscopically observed response expected from a bleach occurring on the nano-grooved surface. Figure 6a shows how the fluorescent image of a bilayer on this surface would look at infinite spatial resolution following a bleach from a Gaussian excitation source. The vertical white stripes in this image are the walls of the grooved surface and reflect the fact these regions have a large number of fluorescent lipids per unit distance in the lateral direction. Fig. 6b shows what this surface would look like when viewed through a 0.45 NA objective with the CCD camera. This image is the convolution of Fig. 6a with a Gaussian Point Spread Function (PSF) that has a standard deviation of 0.5 μm to account for diffraction and CCD pixilation. Lastly, Fig. 6c shows what the underlying concentration profile looks like on an "unfolded" surface following the Gaussian bleach. The "unfolded" surface has a uniform lipid concentration away from the bleach center, but the bleach itself has a banded structure reflecting the presence of the vertical walls of the grooves (note that this latter image is at infinite spatial resolution and has not been convolved with a PSF).

Our simulations start from the image shown in Fig. 6c and use finite time steps and a finite spatial mesh to evolve the concentration profile away from the t=0 value. In our simulation, each spatial grid point (mesh size) is 20 by 20 nanometers. This mesh size is smaller than the features of the grooved surface and, for convenience, is also chosen as a common divisor of all dimensions (a=360 nm, b=320 nm, c=160 nm). The number of fluorescent lipids in

a given mesh point (i,j) is denoted by N_{ij}, with the fluorescence intensity obtained from this point being directly proportional to the number of fluorescent lipids. The number of fluorescent lipids at mesh point i,j following a time step Δt is given by:

$$N_{ij}(t+\Delta t) = N_{ij}(t) + p \cdot \left[N_{i+1j}(t) + N_{i-1j}(t) + N_{ij+1}(t) + N_{ij-1}(t)\right] - 4 \cdot p \cdot N_{ij}(t) \qquad (6)$$

In Equation 6, p is the probability of diffusion of a lipid from one mesh to its nearest neighbor in a time step Δt. The number of fluorescent lipids at the i,j mesh point at $t+\Delta t$, $N_{ij}(t+\Delta t)$, is the number that were there at time t plus the influx of molecules from this mesh point's nearest neighbors minus the efflux of molecules leaving the mesh point due to diffusion. The probability for diffusion out of the grid point in time Δt, p, is directly related to the diffusion coefficient of the lipids as $p=D^*\Delta t/(\Delta x)^2$. These simulations take a finite time step, Δt, of 80 μs, assume a diffusion coefficient of 1 $\mu m^2/s$, and as mentioned above, have a mesh size of Δx = 20 nm. This places the probability of diffusion across a given mesh boundary, p, at 0.2 per 80 μs timestep.

Our simulations diffuse the lipids using the above master equation on the "unfolded" surface (*e.g.*, Figure 6c). The surface is then "refolded" and blurred by a Gaussian PSF to arrive at an image such as that shown in Figure 6b. This procedure creates a series of FRAP images spaced apart in time by 80 μs. We analyze the simulated image every 1000^{th} frame (i.e. every .08 seconds) using the models described in Eqns 1-4. The top panel of Figure 7 shows the simulated FRAP image obtained at t = 1.04 seconds after the bleach (Frame 13000). Below this image are plots of the standard deviations obtained from elliptical Gaussian fits (Eqn 3) to the images as a function of time. The slopes of these lines yields two times the diffusion coefficient for that axis (Eqn 4). The linear fit to the "fast" axis of the Gaussian yields 0.9803 ± 0.0005 $\mu m^2/s$ as the measured diffusion coefficient while the "slow" diffusion axis has an apparent diffusion coefficient of 0.193 ± 0.001 $\mu m^2/s$. The simulated data (Fig. 7) is in good agreement with the measured anisotropic FRAP data (Fig. 4). Moreover, the ratio of the fast to the slow diffusion coefficient on the synthetic data is ~ 5.07, in very good agreement with the ratio expected using the simple approximation laid forth in Eqn 5, ~4.98.

The agreement between the ratio for the diffusion coefficients obtained from the synthetic data (5.07) is closer to the value expected from the simple predictive model (~4.98) than either is to the measured data (~4.3 ± 0.2). Both the simple predictive model and the simulated data assume the substrate is a perfect rectangular structure and that the lipid bilayer is perfectly adherent and conformal to the surface, when realistically, neither of these assumptions are exactly true. As the SEM image of Fig. 1 shows, the underlying surface morphology has some curvature and is not a perfect square well. Moreover, even if the nano-structured surface was perfectly rectangular, a bilayer adhering to this surface would slightly round off the corners, due to the fact there is a minimum radius of curvature to which a bilayer can wrap a tightly curving substrate.[18] Using the models laid forth by Cremer and Boxer[18], the minimum radius of curvature for a POPC bilayer on a silicon oxide surface is ~15 nm, indicating that some softening of tight cornering features could be occurring on these surfaces. This softening of the sharp features, in addition to deviations from ideal square well structure of the underlying substrate, helps to explain the slight discrepancy between the measured ratio of the diffusion coefficients (~4.3 ± 0.2) with the ratio expected either from the simple predictive model, Eqn. 5 (4.98) or that obtained from numerical simulations (5.07).

Conclusions.

In conclusion, we have used a combination of AFM and quantitative fluorescence microscopy to demonstrate the formation of POPC bilayers conformal to a nanotextured surface. These studies illustrate how such membrane architectures may be characterized, and open opportunities for future studies directed at how nanotextured surfaces with tunable physical or chemical properties might be used to influence membrane structure, dynamics and functions. We are planning future studies to address the role of substrate dimensions, the influence of lipid composition, the possible generation of fluid floating layers (in contrast to previously demonstrated bicelle-derived suspended membranes (REF 15), which are essentially laterally immobile), and the use of constructs for the study of biological processes such as cell-surface interactions.

Acknowledgments

This work was performed, in part, at the Center for Integrated Nanotechnologies, a U.S. Department of Energy, Office of Basic Energy Sciences user facility at Los Alamos National Laboratory (Contract DE-AC52-06NA25396) and Sandia National Laboratories (Contract DE-AC04-94AL85000). Add UNM acknowledgment....

Figure Captions.

Figure 1. SEM of nanostructured substrates.

Figure 2. Figure 2. Atomic Force Microscopy of (a) nanostructured substrates alone and (b) nanostructured substrates with a lipid bilayer on the surface. (c) and (d) are cross section profiles of images (a) and (b), respectively.

Figure 3. Fluorescence Recovery after Photobleaching. (a) Fluorescence images obtained at indicated times after initial bleach. The line indicates direction of the grooves of the substrate. (b) Schematic representation indicating diffusion of lipids in two directions.

Figure 4. FRAP data of POPC on grooved silicon. The major and minor axis of the ellipsoidal Gaussian grow at different rates.

Figure 5. An illustration of the nanostructured surface and how one period of this surface (or unit cell) appears if it were "unfolded".

Figure 6. a) A simulation of the fluorescence image from a grooved surface observed with infinite spatial resolution. b) This surface convolved with a Gaussian Point Spread function to account for diffusion and pixilation. c) The simulated bleached image on an "unfolded" surface (see Fig. 5) at infinite spatial resolution.

Figure 7. Top: Simulated FRAP image 1.04 seconds after a bleach. Bottom: fits of the simulated data using Eqns 3 and 4. The "fast" axis of the Gaussian yields an apparent diffusion coefficient of 0.98 mm^2/s while the "slow" diffusion axis has an apparent diffusion coefficient of 0.19 mm^2/s.

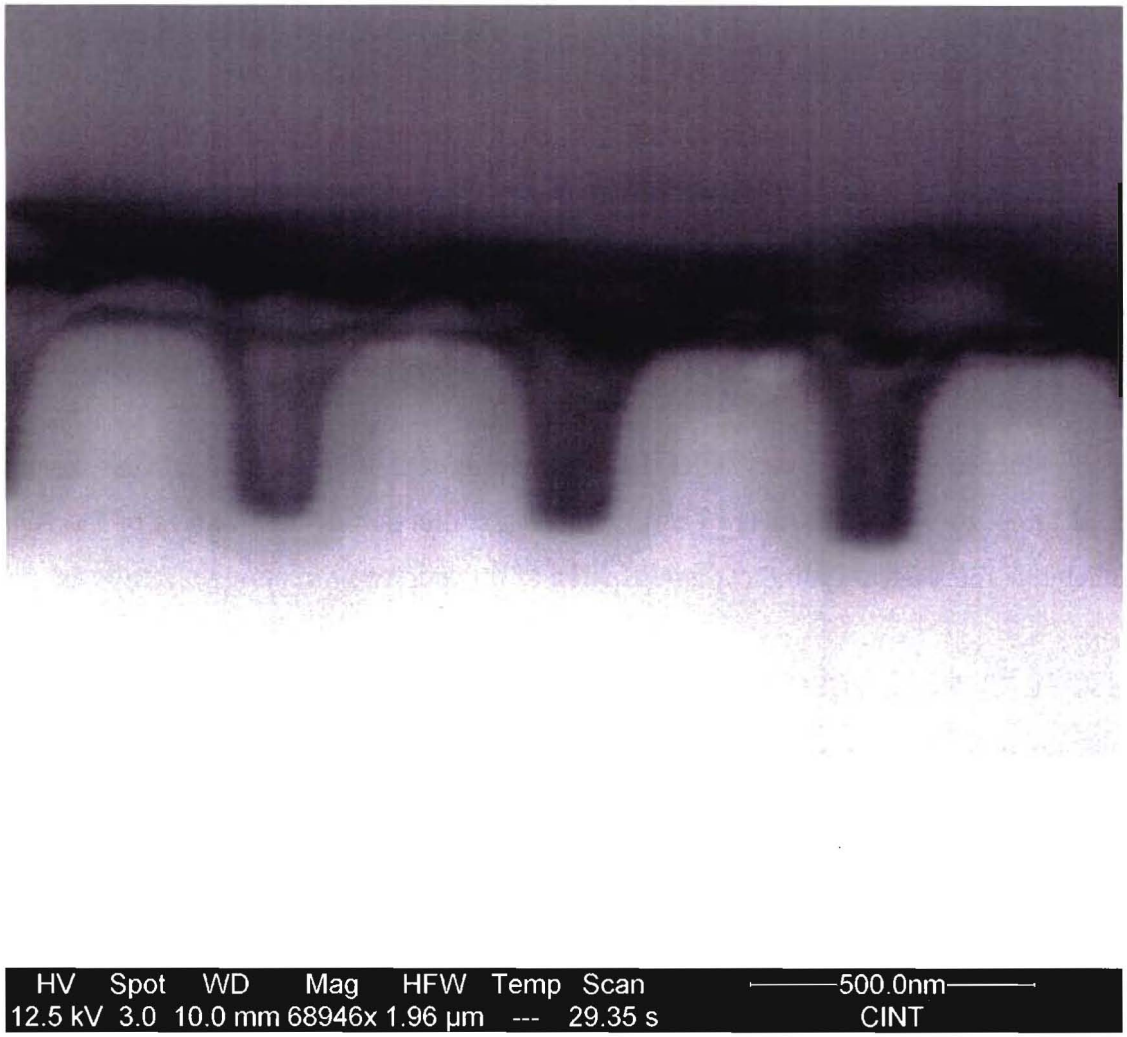
HV Spot WD Mag HFW Temp Scan
12.5 kV 3.0 10.0 mm 68946x 1.96 µm --- 29.35 s
500.0nm
CINT

Figure 1.

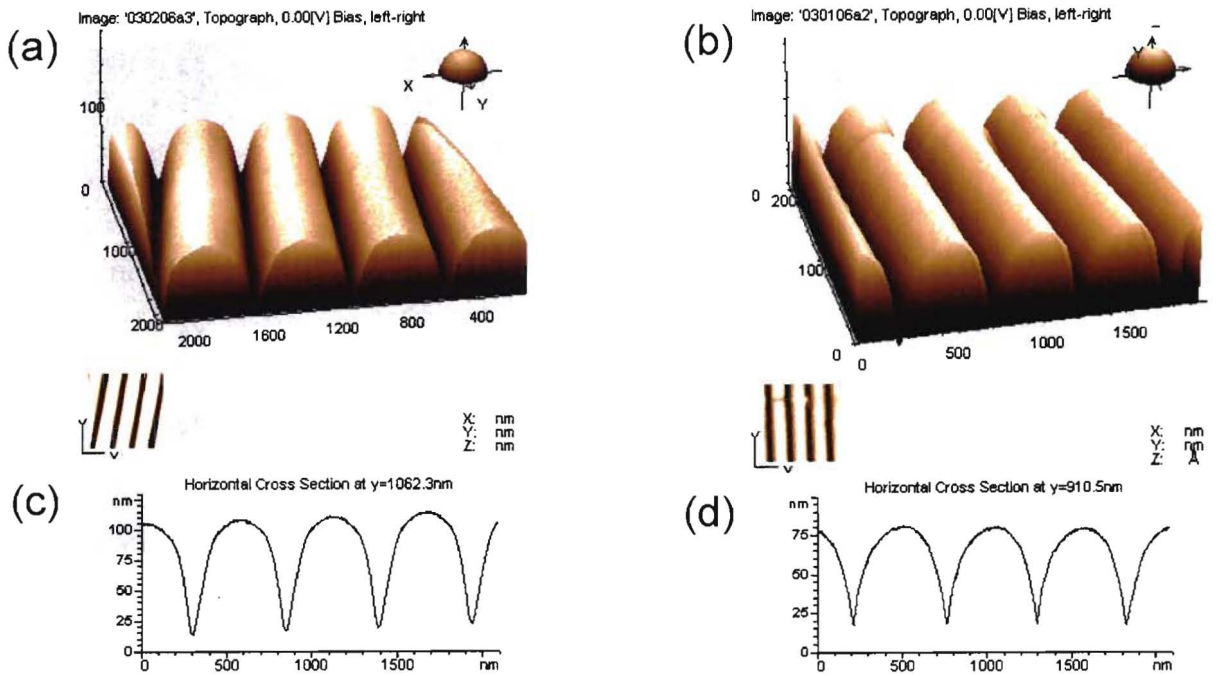
(a)
Image: '030206a3', Topograph, 0.00[V] Bias, left-right
X
Y
100
0
2000
1600
1200
800
400
X: nm
Y: nm
Z: nm
(b)
Image: '030106a2', Topograph, 0.00[V] Bias, left-right
0
500
1000
1500
X: nm
Y: nm
Z: A
(c)
Horizontal Cross Section at y=1062.3nm
nm
100
75
50
25
0
500
1000
1500
nm
(d)
Horizontal Cross Section at y=910.5nm
nm
75
50
25
0
500
1000
1500
nm

Figure 2.

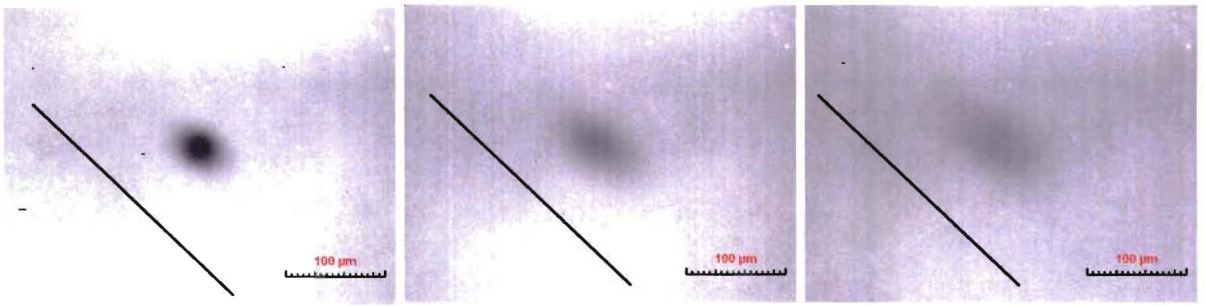

t = 0 min t = 15 min t = 30 min

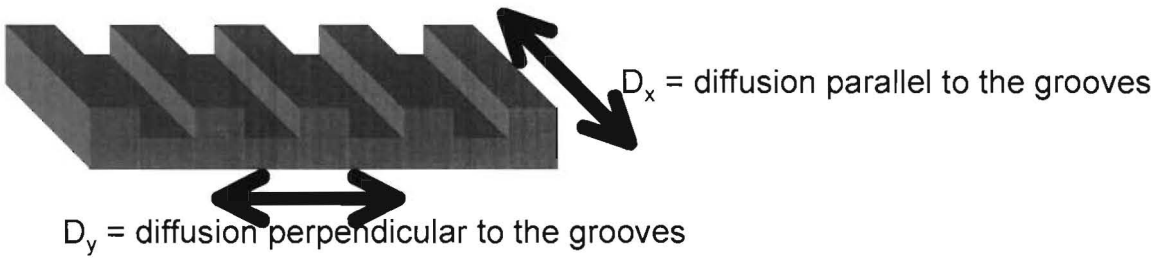

Figure 3.

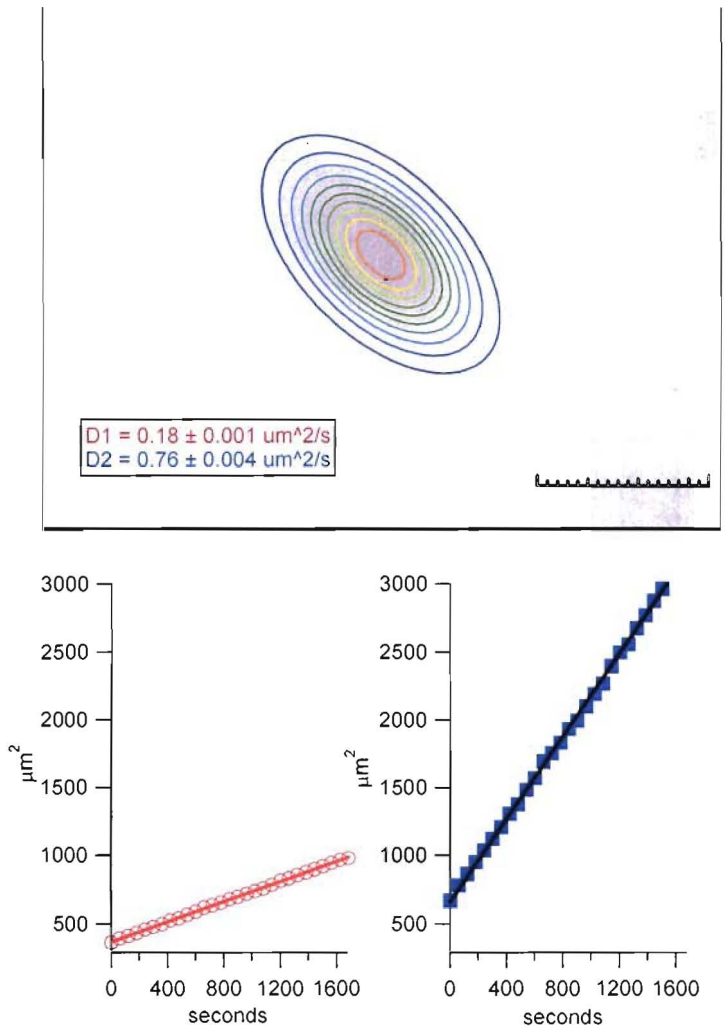
D1 = 0.18 ± 0.001 um^2/s
D2 = 0.76 ± 0.004 um^2/s
3000
2500
2000
1500
1000
500
µm2
0
400
800
1200
1600
seconds
3000
2500
2000
1500
1000
500
µm2
0
400
800
1200
1600
seconds

Figure 4.

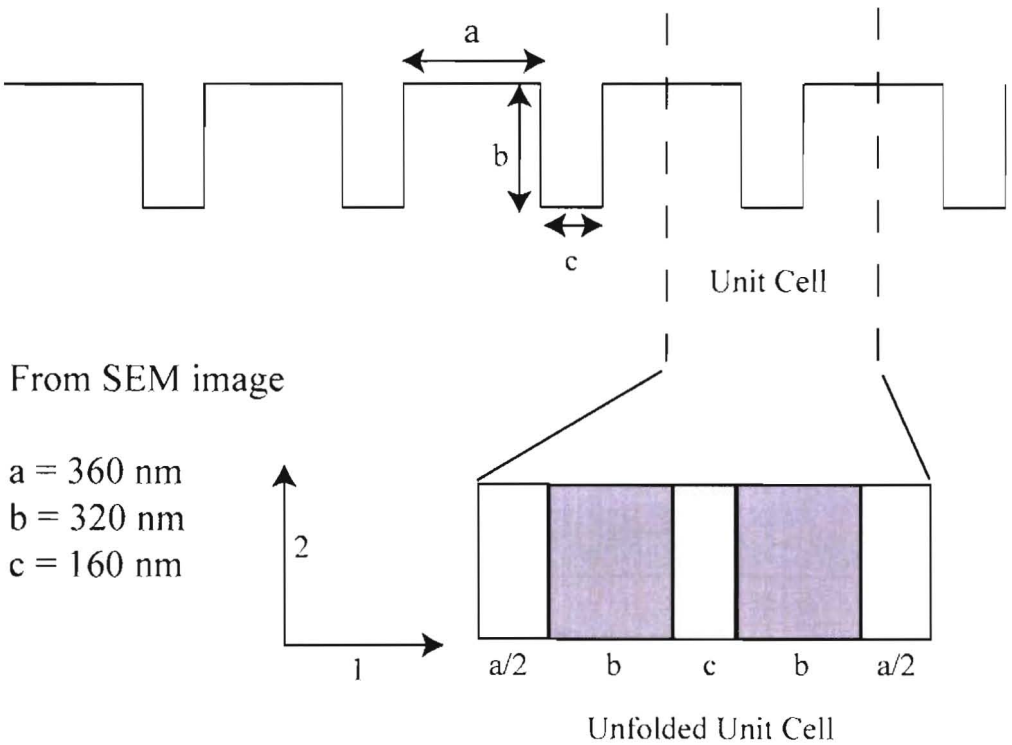
a
b
c
Unit Cell
From SEM image
a = 360 nm
b = 320 nm
c = 160 nm
2
1
a/2
b
c
b
a/2
Unfolded Unit Cell

Figure 5.

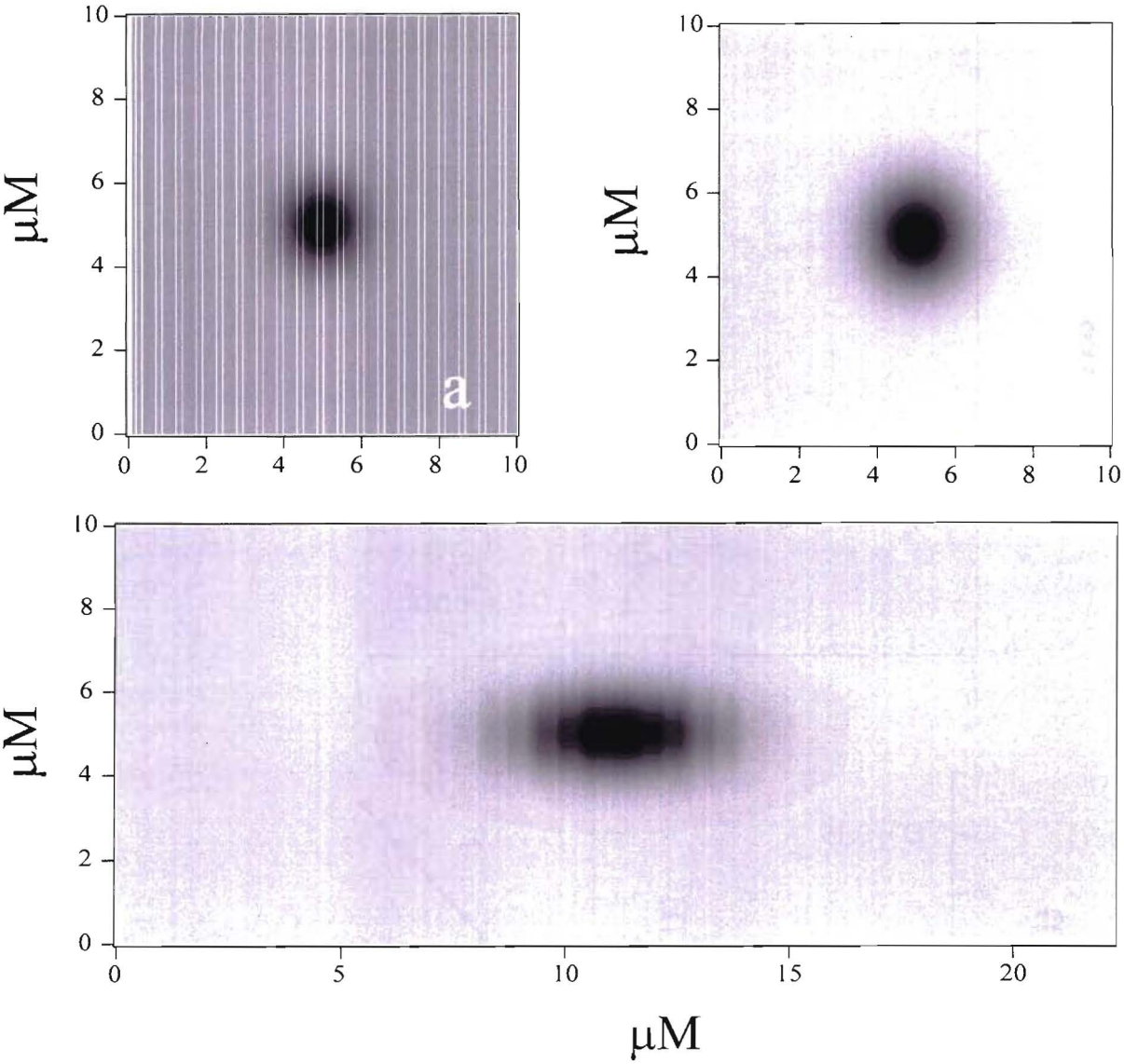

Figure 6.

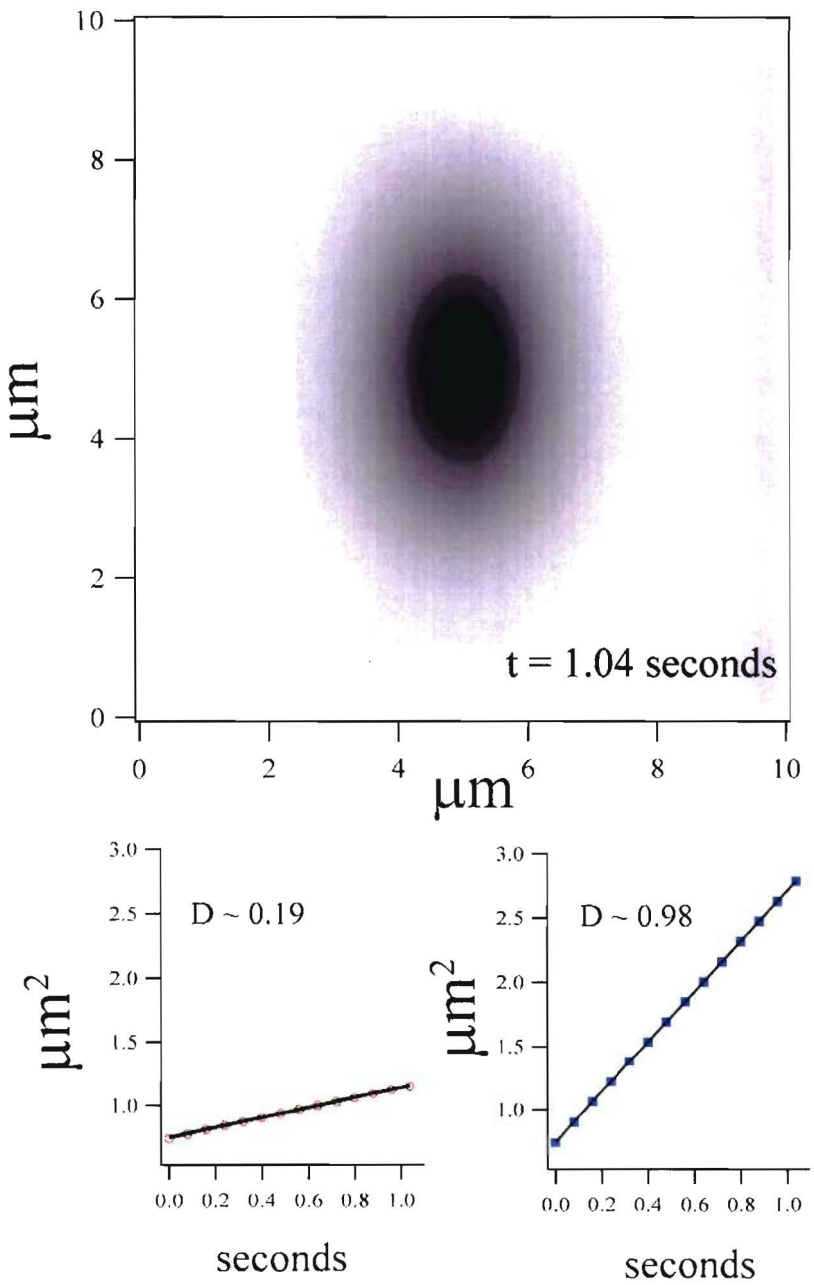
10
8
6
4
2
0
µm
t = 1.04 seconds
0
2
4
6
8
10
µm
3.0
2.5
2.0
1.5
1.0
µm2
D ~ 0.19
0.0 0.2 0.4 0.6 0.8 1.0
seconds
D ~ 0.98
seconds

Figure 7.

References.

1. Tanaka, M.; Sackmann, E., Polymer-supported membranes as models of the cell surface. *Nature* 2005, 437, (7059), 656-63.
2. Daniel, S.; Diaz, A. J.; Martinez, K. M.; Bench, B. J.; Albertorio, F.; Cremer, P. S., Separation of membrane-bound compounds by solid-supported bilayer electrophoresis. *Journal of the American Chemical Society* 2007, 129, (26), 8072-+.
3. Olson, D. J.; Johnson, J. M.; Patel, P. D.; Shaqfeh, E. S. G.; Boxer, S. G.; Fuller, G. G., Electrophoresis of DNA adsorbed to a cationic supported bilayer. *Langmuir* 2001, 17, (23), 7396-401.
4. Groves, J. T., Membrane array technology for drug discovery. *Current Opinion in Drug Discovery & Development* 2002, 5, (4), 606-612.
5. Kung, L. A.; Kam, L.; Hovis, J. S.; Boxer, S. G., Patterning hybrid surfaces of proteins and supported lipid bilayers. *Langmuir* 2000, 16, (17), 6773-6776.
6. Groves, J. T.; Boxer, S. G., Micropattern formation in supported lipid membranes. *Accounts of Chemical Research* 2002, 35, (3), 149-157.
7. Hovis, J. S.; Boxer, S. G., Patterning barriers to lateral diffusion in supported lipid bilayer membranes by blotting and stamping. *Langmuir* 2000, 16, (3), 894-897.
8. Hovis, J. S.; Boxer, S. G., Patterning and composition arrays of supported lipid bilayers by microcontact printing. *Langmuir* 2001, 17, (11), 3400-3405.
9. Lenz, P.; Ajo-Franklin, C. M.; Boxer, S. G., Patterned supported lipid bilayers and monolayers on poly(dimethylsiloxane). *Langmuir* 2004, 20, (25), 11092-11099.
10. Sapuri-Butti, A. R.; Butti, R. C.; Parikh, A. N., Characterization of supported membranes on topographically patterned polymeric elastomers and their applications to microcontact printing. *Langmuir* 2007, 23, (25), 12645-12654.
11. Yee, C. K.; Amweg, M. L.; Parikh, A. N., Membrane photolithography: Direct micropatterning and manipulation of fluid phospholipid membranes in the aqueous phase using deep-UV light. *Advanced Materials* 2004, 16, (14), 1184-1189.
12. Yee, C. K.; Amweg, M. L.; Parikh, A. N., Direct photochemical patterning and refunctionalization of supported phospholipid bilayers. *Journal of the American Chemical Society* 2004, 126, (43), 13962-13972.
13. Howland, M. C.; Sapuri-Butti, A. R.; Dixit, S. S.; Dattelbaum, A. M.; Shreve, A. P.; Parikh, A. N., Phospholipid morphologies on photochemically patterned silane monolayers. *Journal of the American Chemical Society* 2005, 127, (18), 6752-6765.
14. Parthasarathy, R.; Yu, C. H.; Groves, J. T., Curvature-modulated phase separation in lipid bilayer membranes. *Langmuir* 2006, 22, (11), 5095-5099.
15. Zeineldin, R.; Last, J. A.; Slade, A. L.; Ista, L. K.; Bisong, P.; O'Brien, M. J.; Brueck, S. R. J.; Sasaki, D. Y.; Lopez, G. P., Using bicellar mixtures to form supported and suspended lipid bilayers on silicon chips. *Langmuir* 2006, 22, (19), 8163-8168.
16. O'Brien, M. J.; Bisong, P.; Ista, L. K.; Rabinovich, E. M.; Garcia, A. L.; Sibbett, S. S.; Lopez, G. P.; Brueck, S. R. J., Fabrication of an integrated nanofluidic chip using interferometric lithography. *J. Vac. Sci. Technol. B* 2003, 21, 2941-2945.
17. Axelrod, D.; Koppel, D. E.; Schlessinger, J.; Elson, E.; Webb, W. W., Mobility measurement by analysis of fluorescence photobleaching recovery kinetics. *Biophysical Journal* 1976, 16, (9), 1055-69.

18. Cremer, P. S.; Boxer, S. G., Formation and spreading of lipid bilayers on planar glass supports. *Journal of Physical Chemistry B* 1999, 103, (13), 2554-2559.